Two- and three-body effects in single ionization of Li by 95-MeV/u Ar^{18+} projectiles: Analogies with photoionization

N. Stolterfoht, J.-Y. Chesnel, and M. Grether
Hahn-Meitner-Institut Berlin GmbH, Bereich Festkörperphysik, D-14109 Berlin, Germany

J. A. Tanis
Western Michigan University, Kalamazoo, Michigan 49008
and Hahn-Meitner-Institut Berlin GmbH, Bereich Festkörperphysik, D-14109 Berlin, Germany

B. Skogvall*
Technische Universität Berlin, Hardenbergstrasse 36, D-10623 Berlin, Germany

F. Frémont, D. Lecler, D. Hennecart, and X. Husson
Laboratoire de Spectroscopie Atomique, ISMRA F-14050 Caen Cedex, France

J. P. Grandin
Centre Interdisciplinaire de Recherche avec les Ions Lourds, CEA-CNRS, F-14070 Caen Cedex 5, France

Cs. Koncz, L. Gulyás, and B. Sulik
Institute of Nuclear Research (ATOMKI), H-4001 Debrecen, Hungary
(Received 19 August 1998)

Cross sections for single electron emission have been measured in collisions of 95-MeV/u Ar^{18+} projectiles with atomic Li for electron energies ranging from 3 to 1000 eV and angles ranging from 25° to 155°. Models based on the Born approximation are introduced to separate two- and three-body effects in the angular distributions of the ejected electrons. Both experiment and theory provide information about the separability of the two- and three-body effects. The high projectile velocity and the use of the Li target are shown to be essential for the present analysis. The emission of the 1*s* electron is attributed mainly to three-body effects. The cross section for three-body collisions rapidly decreases with the electronic energy transfer involving a power law with an exponent of -3.5. Consequently, two-body effects dominate at high electron emission energies. Remarkably large contributions from two-body collisions were also observed for the low-energy emission of the 2*s* electrons. Demonstrating the analogy in ionization by photons and ions, the two- and three-body processes are associated with Compton scattering and photoabsorbtion, respectively. [S1050-2947(99)05202-6]

PACS number(s): 34.50.Fa, 32.80.Fb

I. INTRODUCTION

Electron emission from a target atom by ion impact has been the subject of intense investigation since the beginning of detailed studies of ion-atom collisions [1,2]. This long-standing interest is due to the fundamental importance of ionization in various fields of physics. Studies of electrons ejected in ion-atom collisions are relevant for numerous applications as well as for basic research of many-body processes [3,4]. The two-body Coulomb problem, involving an ion colliding with a free electron, may be considered as being solved within the framework of quantum mechanics, whereas three-body phenomena can only be described by means of approximate methods. Therefore, the theoretical description of many-body processes remains a challenging task in the field of ion-atom collisions [5]. To help solve this problem it is desirable to separate the two-body part before treating many-body effects. Also, separate studies of the two- and many-body parts provide important insight into the fundamental nature of ionization mechanisms [6–8].

Electron emission spectra exhibit various characteristic features which can be associated with particular ionization mechanisms. Electrons emitted with low energies are particularly important because these electrons have, by far, the largest probability for ejection. These low-energy electrons, referred to as soft-collision electrons, are produced mainly in large impact-parameter collisions. When the velocity of the projectile is much larger than the velocity of the active bound electron, the momentum transfer in a soft collision is very small on an atomic scale. On the other hand, an ejected electron may carry away a significant amount of momentum. When the final electron momentum is larger than the momentum transfer, a third body is required to balance the missing momentum. Hence, if no other particle is ejected in the collision, the target nucleus has to take part in the ionization process. Therefore, soft collisions at high projectile energies can be attributed to three-body collisions involving the projectile, the active electron, and the residual target ion [9,10].

For the case of small momentum transfer, the removal of

*Present address: Friedrich-Ebert-Str. 4, D-15566 Schöneiche, Germany.

an atomic electron by interaction with a fast ion resembles photoionization where the incident photon is annihilated. Similar to a fast ion with small momentum transfer, a photon cannot ionize without the interaction with the residual ion. Hence, photoabsorption necessarily corresponds to a three-body process involving the incident photon, the active electron, and the target ion. The analogy between photons and charged particles with regard to ionization was recognized in the pioneering studies by Bethe [1] and Williams [2] and has subsequently received much attention by Fano [6], Inokuti [7,11], and Kim and collaborators [12,13]. More recently, the construction and use of large ion accelerator facilities and advanced synchrotron light sources have led to new interest in this field [3,5,14–18].

It is well known that the photoeffect is mediated by dipole transitions involving the transfer of a unit angular momentum ($\Delta l=1$). Similarly, a fast ion may be regarded as a source of virtual photons which gives rise to dipole transitions [2]. Due to the uncertainty principle, the angular momentum transfer affects the angular distribution of the ejected electrons. The angular momentum l and the emission angle θ are canonical quantities which are subject to the condition $\Delta l \Delta \theta \gtrsim 1$. Hence, low-order multipole transitions produce a broad angular distribution. In fact, the ejected electrons produced by dipole transitions from an initial s state exhibit a ($\sin^2\theta$)-like angular distribution that is symmetric around 90° [8].

When the projectile is incident in a close encounter with the atomic electron, significant momenta can be transferred in the collision. In such a hard collision, two-body effects become important. The incident ion interacts with an individual electron in a binary-encounter process [19] where the target atom plays only a minor role. The binary-encounter approximation and, thus, the neglect of the interaction with the residual ion are adopted in the framework of the impulse approximation [20,21]. The energy spectra of the binary-encounter electrons exhibit a pronounced peak whose properties are determined by two-body kinematics [4].

As already pointed out by Bethe [1], the two-body process in electron emission by ions is analogous to the Compton scattering of photons. In the latter case, a photon occurs in the final channel of the collision which may provide the missing momentum. Accordingly, as in the case of the binary-encounter process, the target nucleus plays a minor role in the Compton scattering of photons. In addition, from the analogy between ions and photons it is plausible that the shape of the binary-encounter peak is determined by the Compton profile of the corresponding bound orbital [22–24].

A binary-encounter peak occurs in both the energy and angular distributions of the emitted electrons. An important criterion to observe a sharp binary-encounter peak is the validity of the impulse approximation which, in turn, requires projectiles with a large velocity. Fast ions create a binary-encounter peak near 90° in the angular distribution involving high-order multipoles ($\Delta l \gg 1$). The transfer of high angular momenta and the production of a distinct peak of small angular width are consistent with the uncertainty principle mentioned above.

Thus, for fast projectiles two-body effects in ionization produce a sharp peak, while three-body effects give rise to a broad angular distribution of the ejected electrons. These characteristic differences in the angular distributions of the binary- and soft-collision electrons provide an experimental method to separate the two- and three-body effects.

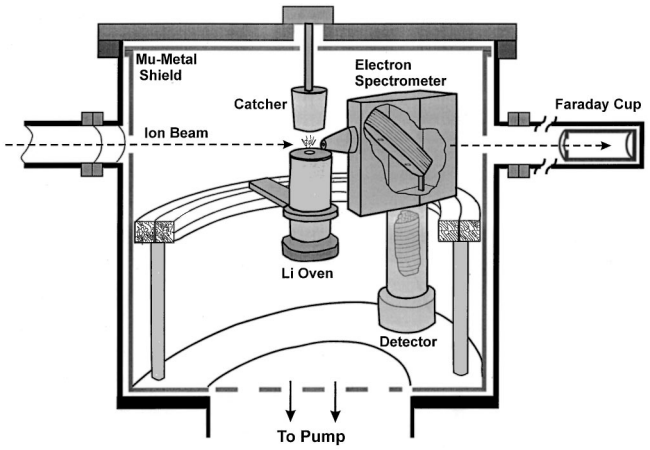

FIG. 1. The experimental setup used to measure angular distribution of electrons ejected in ion-atom collisions. The scattering chamber contains an electron spectrometer and a high-temperature oven producing a vapor target. The spectrometer is mounted on a movable ring. The vapor jet is directed into a cooled catcher.

In preliminary communications we have provided evidence that two- and three-body effects are separable in the angular distributions of electrons ejected in collisions of fast ions with Li [25,26]. It was shown that the two- and three-body effects are quite different for single ionization of $1s$ and $2s$ electrons. This finding has been explained by differences in the binding energies of the electrons as well as in the structures of the corresponding wave functions [4]. It was evident, however, that the analysis required further effort to solve various open questions.

In the present work, we extend our preliminary study [26] of electron emission from Li bombarded with 95 MeV/u Ar^{18+}. The high projectile velocity of nearly half the velocity of light ($v/c=0.42$) is essential for various aspects of the analysis. Atomic Li is shown to provide a unique system to separate two- and three-body effects in the angular distributions of the ejected electrons. Two- and three-body effects are analyzed in terms of the electronic binding energy and the structure of the Li orbitals. The analysis is supported by means of model calculations based on a multipole expansion.

The present study is structured as follows. The experimental and theoretical methods are described in Secs. II and III, respectively. Section IV is devoted to the comparison between experimental and theoretical results. In Sec. V concluding remarks are given. Atomic units are used throughout if not otherwise stated.

II. EXPERIMENTAL METHOD

The measurements were carried out at the GANIL accelerator facility in Caen (France) using the scattering chamber shown in Fig. 1. The essential components in the interior of the scattering chamber are the electron spectrometer and the oven used to produce a lithium vapor jet target. The scattering chamber and the parallel-plate electron spectrometer were similar to those described previously [27]. With this apparatus some preliminary electron spectroscopy experi-

ments with a lithium target were performed earlier [28]. For the present experiments we constructed a new lithium oven which can be heated to high temperature and may be filled with a relatively large quantity of Li [26].

With the amount of ~ 10 g lithium, the oven provided a vapor beam for about 6–8 h with a density corresponding to several mTorr in the target region. The previous high-resolution studies [28] of the Li Auger lines have shown that the target essentially consists of atomic Li, i.e., the fraction of molecular lithium (Li_2) was found to be less than 5%. The center of the collision region was located at a distance of 4 mm from the exit aperture of the oven, which had a diameter of 1 mm. The width of the Li beam in the collision region was estimated to be ~ 5 mm.

When working with the lithium vapor target, various instrumental difficulties had to be solved. The metallic lithium was heated slowly, thereby driving contaminations from the surface, until a stable lithium vapor beam was obtained. For the reliable detection of low-energy electrons, the possibility of perturbing effects due to the electric field resulting from lithium build-up on the spectrometer surfaces must be taken into account. Moreover, when metallic lithium is deposited on insulators separating parts with high voltages, electric breakdowns become likely. To avoid such effects, an efficient baffle system was used to protect the sensitive parts of the spectrometer. Furthermore, magnetic fields associated with the relatively large current (~ 1.5 A) used to heat the metallic lithium had to be expected. To minimize the magnetic fields, the heating wire was used in a bifilar manner. To test for remaining magnetic fields, measurements were taken with the heating current on and off and no changes in the electron spectra could be detected. With the present spectrometer setup, electron yields could be measured reliably for emission energies as low as ~ 3 eV.

The Li vapor target was crossed by a beam of 95-MeV/u Ar^{18+} ions whose current was $1-2\,\mu$A. The beam was collimated to a size of about 2 mm $\times$ 2 mm. Continuum electrons emitted from the Li target were analyzed with the spectrometer within the electron energy range from about 3 to 1000 eV. The spectrometer had a solid angle of about 10^{-3} sr and a relative energy resolution of 5.5%. Ejected electrons were observed in an angular range from 25° to 155° which was scanned in relatively small steps. The maximum of the binary-encounter peak in the vicinity of 90° was measured with an angular step size of 2° and in the wings of the peak the step size was 5° to 10°.

From the measured electron intensities we determined cross-sections differential in the energy and angle of the ejected electrons. To obtain absolute cross sections we integrated the measured data over the electron emission angle and normalized the results to the corresponding Rutherford cross section [3,4]. This was done at one energy point near 200 eV for the part of the spectrum produced by two-body effects (see also below). The relative errors with respect to a variation of the electron energy and angle are about $\pm 25\%$. At energies below ~ 10 eV the experimental uncertainties increase and reach about $\pm 40\%$ at the lowest energy measured (3 eV).

Typical double-differential cross-section spectra are shown in Fig. 2 as a function of the electron energy for the electron emission angles of 25°, 65°, and 90°. The spectra

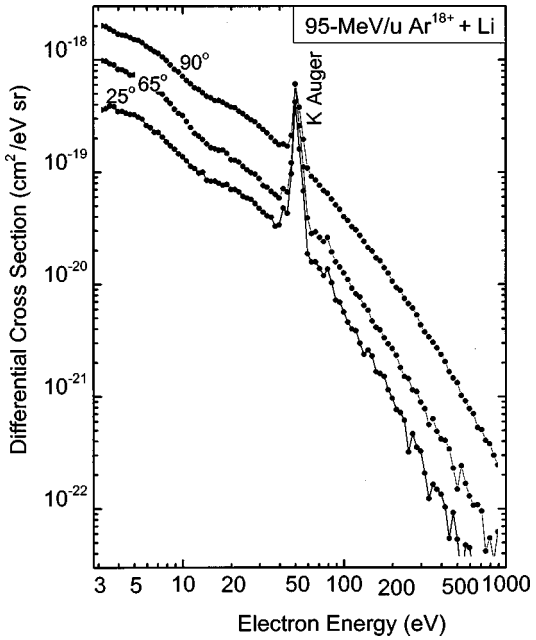

FIG. 2. Energy distributions of electrons emitted in collisions of 95-MeV/u Ar^{18+} on Li at angles of 25°, 65°, and 90°. The continuum part of the electron spectra originates from single ionization of the Li target. The peak at 52 eV is due to *KLL* Auger electrons ejected after exciting a $1s$ electron to a higher bound state.

show a distinct maximum at about 52 eV which is due to *KLL* Auger transitions in core excited lithium. The Auger spectra contain several lines [28] from which the most intense one is attributed to the initial configuration $1s2s2p$. Furthermore, the cross sections for continuous electron emission increase strongly with increasing angle up to 90°, where the data reach a maximum indicating the occurrence of the binary-encounter peak.

It is noted that the measured data represent the sum of the electron emission from both the $1s$ and $2s$ orbitals. The individual contributions from these shells will be separated by means of model calculations as outlined in the following section.

III. THEORETICAL ANALYSIS

The fast collisions relevant in this work are treated by means of perturbation theory. For 95-MeV/u Ar^{18+} the ratio of projectile charge to projectile velocity is equal to $Z_p/v_p \approx 0.3$. This interaction parameter is expected to be sufficiently small for the validity of the Born approximation [4]. Nevertheless, to ensure that two-center effects are negligible, we evaluated electron emission cross sections from the continuum-distorted wave (CDW-EIS) code by Gulyás *et al.* [29] in comparison with corresponding Born-approximation calculations using the same code. The higher-order contributions were found to be less than a few percent so that they could be neglected in the present analysis.

Within the framework of the Born approximation, the double-differential cross section for emission of electrons with energy ϵ into the solid angle Ω is given by [7]

$$\frac{d\sigma}{d\epsilon\, d\Omega} = 4Z_p^2 M^2 \frac{K_f}{K_i} k \int_{K_{\min}}^{K_{\max}} \frac{|F_{if}(\mathbf{K})|^2}{K^4} d\Omega_f, \qquad (1)$$

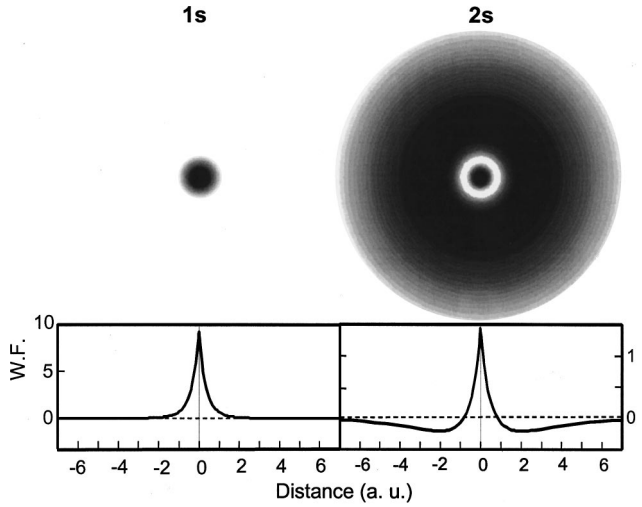

FIG. 3. Electron densities (upper part) and wave functions (lower part) for the atomic orbitals $1s$ and $2s$ of Li evaluated using the Cowan code [30]. From [26].

where Z_p and M are the projectile charge and the reduced mass, respectively, $\mathbf{K}=\mathbf{K}_f-\mathbf{K}_i$ is the momentum transfer, with K_i and K_f being the initial and final projectile momenta, and $k=\sqrt{2\epsilon}$ is the momentum of the ejected electron. The integration is performed over the solid angle $d\Omega_f = \sin\theta_f\ d\theta_f\ d\varphi_f$ of the scattered projectile, where the momentum transfer is subject to the condition $K=(K_i^2+K_f^2 - 2K_iK_f\cos\theta_f)^{1/2}$ involving the projectile scattering angle θ_f. The minimum momentum transfer $K_{\min}$ is obtained as

$$K_{\min}\approx\frac{\Delta E}{v_p}, \tag{2}$$

where ΔE is the energy transfer and v_p the projectile velocity. The maximum momentum transfer is given by $K_{\max}\approx 2v_p$. Moreover,

$$F_{if}(\mathbf{K})=\int \varphi_f^*(\mathbf{r})\mathbf{e}^{-i\mathbf{K}\cdot\mathbf{r}}\varphi_i(\mathbf{r})d\mathbf{r} \tag{3}$$

is the atomic form factor, where φ_i and φ_f are the initial and final states of the active electron, respectively.

Since the electronic structures of the initial Li states φ_i are important for the present analysis [26], we exhibit the densities and wave functions [30] of the bound orbitals $1s$ and $2s$ in Fig. 3. The $1s$ electron has a binding energy of about 59 eV and is localized close (<1 a.u.) to the nucleus. The $2s$ electron has a much smaller binding energy of about 5.5 eV. Due to the node in the wave function, the $2s$ orbital has two parts, an inner part close to the nucleus (<1 a.u.) and an outer part extending quite far from the nucleus (up to about 7 a.u.).

For various applications it is useful to expand the form factor over the final angular momentum states. This has been done in the early work by Madison *et al.* [31] and Manson *et al.* [32] to allow for the use of numerical wave functions φ_i and φ_f. In the present work, such an expansion is applied to study individual multipole terms. The corresponding expansion is given by

$$F_{if}(\mathbf{K})=\sum_{lm} F_{lm}(\mathbf{K})Y_{lm}(\Omega), \tag{4}$$

where Y_{lm} are spherical harmonics for the angular momentum l and magnetic quantum number m of the final state. In the following, $l=\Delta l$ since initial s states are used. Then the form factor $F_{lm}(\mathbf{K})$ can be expressed as

$$F_{lm}(\mathbf{K})=\sqrt{4\pi}e^{i\delta_l}Y_{lm}(\Omega_K)f_{\epsilon ln}(K), \tag{5}$$

where $f_{\epsilon ln}(K)=\int R_{\epsilon l}(r)j_l(Kr)R_{ns}(r)r^2dr$ is the radial matrix element containing a Bessel function j_l and the radial wave functions R_{ns} and $R_{\epsilon l}$ associated with φ_i and φ_f, respectively. The solid angle Ω_K specifies the direction of the momentum transfer.

Thus, a coherent sum of multipoles is obtained,

$$\frac{d\sigma}{d\epsilon\ d\Omega}=4Z_p^2M^2\frac{K_f}{K_i}k\int_{K_{\min}}^{K_{\max}}\left|\sum_{lm}\frac{F_{lm}(\mathbf{K})}{K^2}Y_{lm}(\Omega)\right|^2 d\Omega_f \tag{6}$$

which can be evaluated introducing a multiple sum over l, l', m, and m'. The integration over azimuthal angle $d\varphi_f$ of the solid angle $d\Omega_f=\sin\theta_f\ d\theta_f\ d\varphi_f$ gives rise to the constraint $m=m'$. The polar angle $d\theta_f$ can be expressed in terms of the momentum transfer, i.e., $\sin\theta_f d\theta_f=(K_iK_f)^{-1}K\,dK$. Thus, after regrouping the diagonal ($l=l'$) and nondiagonal ($l\neq l'$) terms, one obtains

$$\frac{d\sigma}{d\epsilon\, d\Omega}=8\pi\frac{Z_p^2}{v_p^2}k\left\{\sum_{lm} b_{lm}|Y_{lm}(\Omega)|^2 + \sum_{l\neq l'm} c_{ll'm}Y_{lm}^*(\Omega)Y_{l'm}(\Omega)\right\}, \tag{7}$$

where the coefficients

$$b_{lm}=\int_{K_{\min}}^{K_{\max}}\frac{|F_{lm}(\mathbf{K})|^2}{K^3}dK \tag{8a}$$

and

$$c_{ll'm}=\int_{K_{\min}}^{K_{\max}}\frac{F_{lm}^*(\mathbf{K})F_{l'm}(\mathbf{K})}{K^3}dK \tag{8b}$$

govern the contributions of individual angular momenta and their interferences, respectively. Due to the orthogonality of the spherical harmonics, the interference terms cancel when single-differential cross sections are evaluated by integrating over the electron observation angle.

We calculated individual multipole terms relevant for integrated cross sections within the framework of the Born approximation using a program similar to that of Gulyás *et al.* [29]. The program implies Hartree-Fock-Slater wave functions for the initial and final state of the active electron. Figure 4 shows examples for the quantity $|F_{lm}(K)|^2/K^3$ occurring within the integral of Eq. (8a). (After a summation over m, the vector $\mathbf{K}$ reduces to the modulus K.) Results are given for the angular momenta $l=1$ and $l\neq 1$ showing that the function $|F_{lm}(K)|^2/K^3$ maximizes in different ranges of

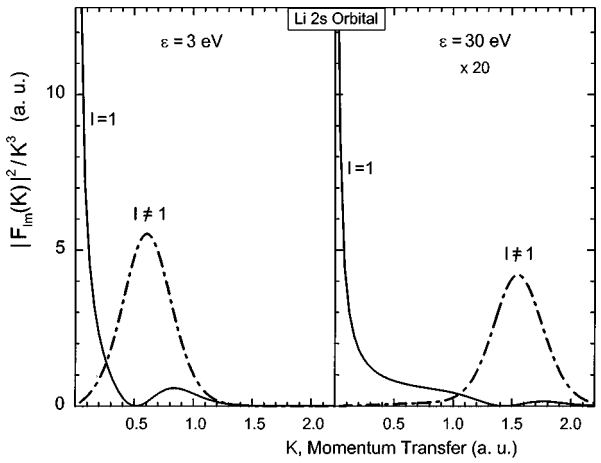

FIG. 4. Expression $|F_{lm}(K)|^2/K^3$ for the Li $2s$ orbital summed over m for the angular momenta $l=1$ and $l\neq 1$ as a function of the momentum transfer K. The left-hand side is for 3 eV electrons and the right-hand side for 30 eV. For the convenient graphical display the 30 eV data are multiplied by a factor of 20. The data are calculated by means of the Born approximation using a program similar to that of Gulyas *et al.* [29].

the momentum transfer. The $l=1$ contribution is strongly peaked at $K\rightarrow 0$, whereas the contribution of the $l\neq 1$ multipoles exhibits a maximum near $K\approx k$ whose low-energy wing falls off rapidly at $K\rightarrow 0$. The occurrence of two distinct peaks in K space supports the separation of the $l=1$ and $l\neq 1$ multipoles.

The separation of the form factor has already been proposed in the pioneering work of Bethe [1]. To allow individual treatments of small and large momentum transfers, Bethe [1] introduced an intermediate momentum transfer K_0 to split the integral in Eq. (1),

$$\frac{d\sigma}{d\epsilon\ d\Omega}=8\pi\frac{Z_p^2}{v_p^2}k\left\{\int_{K_{\min}}^{K_0}\frac{|F_{if}(\mathbf{K})|^2}{K^3}dK+\int_{K_0}^{K_{\max}}\frac{|F_{if}(\mathbf{K})|^2}{K^3}dK\right\}. \tag{9}$$

In various studies [1,3,7,12] the first term in Eq. (9) has been recognized as being due to dipole transitions ($l=1$). As seen from Fig. 4, the intermediate momentum transfer K_0 may be located at the minimum of the $|F_{lm}(K)|^2/K^3$ curve, i.e., at the crossing point of the $l=1$ and $l\neq 1$ curves. Thus, the multipoles can be separated in good approximation and, indeed, the first term is nearly exclusively attributed to dipole transitions. Since the $l\neq 1$ peak maximizes near $k=\sqrt{2\epsilon}$, the two peaks approach each other with decreasing energy ϵ and their overlap may become significant. However, Fig. 4(a) indicates that even the results for the lowest energy (3 eV) provide confidence that the groups due to $l=1$ and $l\neq 1$ can be fairly well separated.

Bethe [1] has also drawn the attention to the analogy between ionization by ions and photons. The dipole term corresponds to photoabsorption where a photon is annihilated and the second term corresponds to the Compton effects where a photon remains in the final state. As pointed out above, photoabsorption cannot occur without the interaction with the target nucleus and, hence, photoabsorption is necessarily a three-body process. On the other hand, the Compton effect may proceed without the presence of the target nucleus so that the two-body aspect becomes dominant. Accordingly, in ion-atom collisions the distinction of the $l\neq 1$ and $l=1$ contributions is associated with the separation of two- and three-body effects, respectively. We recall that this separation is primarily justified by the different K dependencies of the form factors given in Fig. 4.

In the following we shall deduce approximate expressions for the two- and three-body parts which can be used to calculate the corresponding contributions. The cross sections due to the two- and three-body parts will be specified by the labels 2 and 3, respectively. First, we treat the three-body part by using the dipole term for $l=1$ from Eq. (7). Hence, the angular distribution reduces to $A+B\sin^2\theta$, where the constants A and B are given by the coefficients b_{10} and $b_{1\pm 1}$ from Eq. (8a). Since the smooth component of the experimental angular distribution (three-body part) exhibits asymmetries, we also keep the monopole term $l=0$ which modifies the constant A and introduces the cross term $C\cos\theta$ with $C=c_{100}$ due to an interference effect with the dipole term. Hence one obtains

$$\frac{d\sigma_3}{d\epsilon\ d\Omega}=A+B\sin^2\theta+C\cos\theta. \tag{10}$$

As will be shown below, the monopole term is small due to the high projectile energy used in this work. Furthermore, it is recalled from Eq. (7) that the interference term is subject to the constraint $m=m'$. At high impact energies the dipole term with the magnetic quantum number $m=1$ dominates so that the interference with the monopole term ($m=0$) is small. As the monopole term and the related interference are not significant, the sum of monopole and dipole terms will be referred to as an extended dipole term. For small interferences it can be seen from Eq. (10) that the three-body part of the electron emission cross section has a broad angular distribution governed by the $\sin^2\theta$ term.

The two-body part refers to the second term in Eq. (9) representing the transfer of high momenta and angular momenta characteristic for violent collisions. For such a case it is reasonable to treat ionization as a binary collision between the incident particle and the target electron while neglecting the target nucleus. Within this treatment, referred to as the impulse approximation [20], the momentum balance is given by $\mathbf{p}=\mathbf{k}-\mathbf{K}$, where $\mathbf{p}$ is the initial momentum of the bound electron. Moreover, the final state of the electron is described by a plane wave $\varphi_f=(2\pi)^{-3/2}e^{-i\mathbf{k}\cdot\mathbf{r}}$ so that the form factor from Eq. (3) can be identified with the initial wave function in momentum space,

$$\tilde{\varphi}_i(\mathbf{p})=\frac{1}{(2\pi)^{3/2}}\int \mathbf{e}^{-i\mathbf{p}\cdot\mathbf{r}}\varphi_i(\mathbf{r})d\mathbf{r}. \tag{11}$$

For further evaluation the solid angle of the scattered particle $d\Omega_f\approx(K_iK_f)^{-1}d^2K_\perp$ is written in terms of the momentum transfer $\mathbf{K}_\perp$ perpendicular to the incident beam direction $\mathbf{K}_i$. Hence, the double-differential cross section for two-body collisions is obtained as (Bell *et al.* [22])

$$\frac{d\sigma_2}{d\varepsilon\, d\Omega}=4\frac{Z_p^2}{v_p^2}k\int_{K_0}^{K_{\max}}\frac{|\tilde{\varphi}(\mathbf{K})|^2}{K^4}d^2K_\perp . \tag{12}$$

The momentum distribution $|\tilde{\varphi}_i(\mathbf{p})|^2$ represents a distinct peak, which corresponds to the $l\neq 1$ peak shown in Fig. 4. Hence, to simplify Eq. (12) one may perform a peaking approximation [4,33] by setting K equal to an effective value k_c, which is close to the maximum location of the $l\neq 1$ peak in Fig. 4.

The quantity k_c may be approximated by the mean value of the momentum transfer K. Recalling that $K^2=k^2+p^2-2k\,p\cos\beta$ and assuming that the cross term is canceled by the averaging procedure, we set

$$k_c\approx(k^2+\overline{p^2})^{1/2}, \tag{13}$$

where $\overline{p}$ is the mean value of the initial momentum distribution of the electron. In accordance with the virial theorem, the mean momentum of the electron may be deduced from its binding energy E_b, i.e., we set $\overline{p}=c\sqrt{2E_b}$, where $c=1.2$ is the correction factor for multielectron atoms [3]. Moreover, in binary collisions the kinetic energy ϵ may be replaced by the energy transfer $\Delta E=\epsilon+E_b$ [9] and, accordingly, the momentum k by k_c in a good approximation.

Finally, one obtains for the double-differential cross section

$$\frac{d\sigma_2}{d\epsilon\, d\Omega}=\frac{4Z_p^2}{v_p^2k_c^3}J(p_z), \tag{14}$$

where

$$p_z=k\cos\theta-K_{\min} \tag{15}$$

is the initial momentum component along the beam direction and $J(p_z)=\int|\tilde{\varphi}_i(\mathbf{p})|^2\,d^2p_\perp$ is the Compton profile of the initial state. The integration variable $\mathbf{K}_\perp$ was substituted by the component $\mathbf{p}_\perp$ of the initial momentum perpendicular to the incident beam direction. It should be pointed out that the peaking approximation suppresses the dipole term, so that the lower integration limit for $\mathbf{p}_\perp$ may be set to zero in a good approximation. In the following, the method yielding Eq. (14) is referred to as the *free-electron peaking approximation* (FEPA) [4].

Taking into account the normalization of the Compton profile, $\int J(p_z)dp_z=1$, the FEPA formula (14) may readily be integrated over the solid angle, yielding the simple expression

$$\frac{d\sigma_2}{d\epsilon}=\frac{2\pi Z_p^2}{v_p^2\,\Delta E_c^2} \tag{16}$$

with $\Delta E_c=k_c^2/2=\epsilon+c^2E_b$. A similar expression has previously been deduced from the Rutherford cross section [3,4] using ΔE instead of ΔE_c. The differences resulting from this replacement are significant for $\epsilon\to 0$, but vanish for $\epsilon\gg E_b$.

Returning to the double-differential cross sections, we note that Eq. (14) describes a distinct peak which is identified as the binary-encounter peak. It can readily be shown that the location of the binary-encounter peak is determined from the condition that the Compton profile maximizes at $p_z=0$. For the electron energy at the binary-encounter maximum it follows that (Fainstein *et al.* [34])

$$\epsilon_{\mathrm{BE}}=2v_p^2\cos^2\theta-2E_b . \tag{17}$$

This formula indicates that the electrons are ejected near 90° when the electron velocity remains much lower than the projectile velocity. The latter condition can readily be achieved when high-velocity projectiles are used.

Since angular distributions of the ejected electrons are of primary interest here, we estimate the angular width from Eq. (15) forming the derivative $dp_z/d\theta=k\sin\theta$. Thus, the width of the binary-encounter peak is obtained as

$$\Delta\theta\approx\frac{\Delta p_z}{k\sin\theta}. \tag{18}$$

It is recalled that high-velocity projectiles eject electrons primarily at angles $\theta\approx 90°$. Hence, $\sin\theta$ reaches its maximum value of unity and the angular width $\Delta\theta$ reaches its minimum, i.e., the binary-encounter peak is relatively sharp when produced by high velocity projectiles.

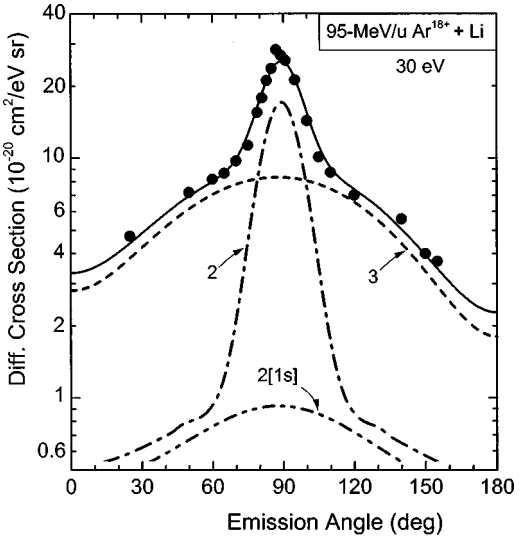

FIG. 5. Angular distribution of 30 eV electrons emitted in collisions of 95-MeV/u Ar^{18+} on Li. The dot-dashed curve labeled 2 refers to calculations using the two-body theory given by Eq. (14). The dot-dot-dashed curve labeled $2[1s]$ refers to the two-body part from the $1s$ orbital only. The dashed curve labeled 3 is a fit to the underlying three-body part using the extended dipole term $A+B\sin^2\theta+C\cos\theta$ (see text). The solid curve is the sum of all contributions.

IV. DISCUSSION OF THE RESULTS

In order to verify the contributions from two- and three-body processes, we compare the experimental and theoretical results for angular distributions of the ejected electrons. An example for 30 eV electrons is given in Fig. 5. The two-body part is evaluated by means of Eq. (14) where the Compton profiles were deduced from atomic Hartree-Fock wave functions [30]. Figure 5 shows the fraction for the $1s$ shell (la-

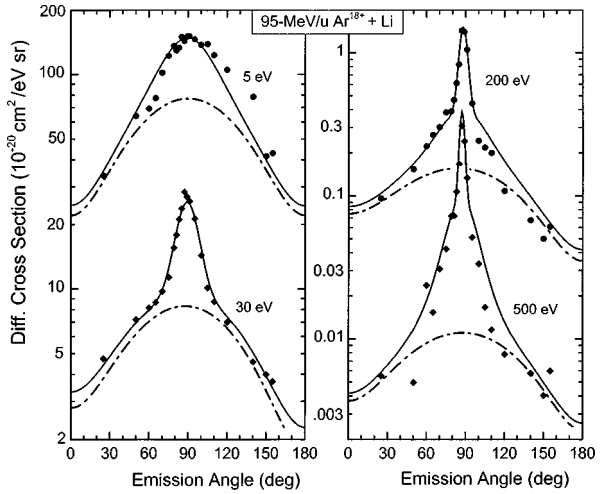

FIG. 6. Angular distributions of electrons emitted in collisions of 95-MeV/u Ar^{18+} on Li at energies of 5, 30, 200, and 500 eV. The dot-dashed curve is a fit to the underlying three-body part using the extended dipole term $A+B\sin^2\theta+C\cos\theta$ (see text). The solid curve is the sum of the two- and three-body parts.

beled $2[1s]$) and the total two-body contribution (labeled 2) including both the $1s$ and $2s$ shells. After subtraction of the two-body part, the extended dipole term Eq. (10) is used to fit the experimental data taken primarily at forward ($\leqslant 60°$) and backward angles ($\geqslant 120°$). The result of the fit (labeled 3) is given by the dashed curve and the sum of all the theoretical components is given by the solid curve.

A. Two-body phenomena

In Fig. 5 the most significant feature of the spectrum is the distinct binary-encounter peak near 90° which represents the two-body processes. As outlined in Sec. III, the shape of the binary-encounter peak is determined by the Compton profile of the target electrons. An important consequence of the Compton profile analysis by means of Eq. (14) is that the most distinct part of the binary-encounter peak can be attributed to the $2s$ orbital. The $1s$ electron, since it involves higher momenta, has a broader Compton profile as can be seen from the $2[1s]$ curve. Also, the inner part of the $2s$ wave function, since it is closer to the nucleus (Fig. 3), produces a broader component in the Compton profile. In fact it is found that, apart from a constant factor, the Compton profiles for the $1s$ wave function and the inner part of the $2s$ wave function are essentially equal. Thus, the $1s$ wave function as well as the effect of the node in the $2s$ orbital give rise to a ''kink'' in the Compton profile, which is clearly confirmed by the experiment.

More examples for energies of 5, 30, 200, and 500 eV are given in Fig. 6. For reasons of graphical display we show only the three-body part and the total sum of the model calculations. The model results are seen to agree well with the experimental data. The only significant deviations between the model and experiment occur in the region of backward angles; e.g., see the data for 200 eV. These deviations cannot be accounted for by an increased interference between the dipole and monopole term (the corresponding cross sections would have to become negative above $\sim 155°$). Rather, the observed discrepancy is attributed to the interference between the dipole ($l=1$) and higher multipoles such as the quadrupole ($l=2$). In the angular distributions of the emitted electrons, the interference between these multipoles may cause ambiguities in the separability of the two- and three-body effects. However, as shown later, the different multipoles are fully separable in the single differential cross sections.

The distinct part of the binary-encounter peak is found on top of a broader maximum [altogether superimposed on the $(\sin^2\theta)$-like dipole curve]. Again, this broader maximum is associated with the two-body contribution of the $1s$ orbital and the inner part of the $2s$ orbital. The relative importance of these contributions changes with electron energy. The inner part of the $2s$ wave function contributes primarily at lower electron energies, while the two-body contribution of the $1s$ orbital becomes more important at higher energies $\gtrsim 100$ eV. Another feature of the spectra in Fig. 6 is that the binary-encounter peak becomes more and more narrow at higher electron energies. This increasing sharpness of the Compton profile may readily be understood from Eq. (18) yielding for the angular width $\Delta\theta=\Delta p_z/k$ when setting $\sin\theta\approx 1$ at angles near 90°. Hence, for a given Δp_z it follows that the angular width $\Delta\theta$ decreases with increasing electron momentum k.

The results in Fig. 6 show that the two- and three-body parts change considerably in magnitude with varying electron energy. For higher electron energies (e.g., 500 eV) the two-body processes account for nearly all of the electron emission. At lower energies, however, the two-body part does not vanish. For 5 eV electrons the two-body contribution is still nearly as large as the three-body part. This finding is remarkable. Since the pioneering work of Bethe [1] it has become common practice to attribute the emission of low-energy electrons by fast projectiles to three-body dipole transitions [7,12]. The present experiments, however, show that significant contributions due to two-body processes remain at the low-energy limit.

To study further the properties of the two-body interaction, theoretical results for individual multipoles were evaluated within the framework of the first Born approximation (B1) using a modified version of the program by Gulyás *et al.* [29]. The calculated double-differential cross sections were integrated over the electron emission angle. As mentioned, the angular integration cancels the interferences between multipoles (e.g., dipole and quadrupole) so that the multipole terms become fully separable. The results for the single differential cross section involving all multipoles with $l>1$ are shown in Fig. 7(a). As discussed in the theoretical section, these multipoles represent essentially the two-body contributions. Moreover, experimental two-body contributions were obtained by integration of the double-differential cross sections after subtraction of the corresponding three-body parts represented by the dot-dashed curve in Fig. 6.

In addition, Fig. 7 shows results from the simple formula (16) derived above from the FEPA model. Apart from discrepancies at lower energies, where the FEPA is not expected to yield accurate results, the two theoretical data sets exhibit excellent agreement. This agreement is remarkable in view of the simplicity of the FEPA model, which includes no adjustable parameters. As mentioned in Sec. II, the FEPA formula (16) was used to normalize the experimental cross

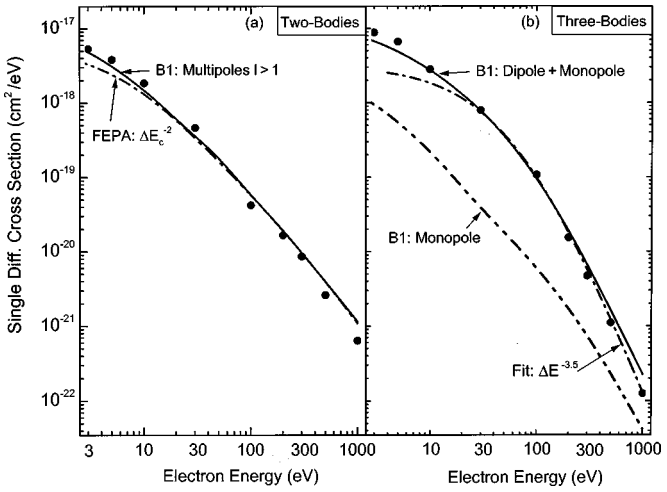

FIG. 7. Angle-integrated cross sections for electron emission in 95-MeV/u $Ar^{18+}+Li$ collisions separated into two-body processes (a) and three-body processes (b). In (a), the experimental data points were obtained by integrating the measured angular distributions after subtraction of the three-body part, shown in (b). The curve labeled ''B1'' was evaluated for the multipoles $l>1$ by means of the Born approximation using the code by Gulyás *et al.* [29]. The curve labeled ''FEPA'' refers to formula (16). In (b) the experimental data points originate from the fits of Eq. (10) to the experimental results shown in Fig. 6. The curves labeled ''B1'' were evaluated using the Born approximation [29]. The dash-dot-dot line labeled ''Monopole'' refers to monopole ($l=0$) transitions. The full line labeled ''Dipole+Monopole'' refers to dipole ($l=1$) plus monopole transitions. The dash-dot line labeled ''Fit'' represents the function $x\Delta E^{-3.5}$ where ΔE is the electronic energy transfer and x is a fit parameter adjusted to achieve the best agreement with experiment (see text).

sections. For the normalization all experimental data were multiplied with a single factor which was adjusted to achieve agreement with theory near 200 eV. For higher electron energies it should be pointed out that the experimental results are underestimated by numerical integration problems due to the finite step size in the angular distribution measurements.

The present results show that the FEPA model is an excellent tool to describe the two-body part of the Li ionization mechanism. Similar conclusions have been drawn by Bell *et al.* [22] for other target species; see also the work by Zouros *et al.* [24]. For the following discussion of three-body effects it should be kept in mind that the FEPA formula (16) implies a ΔE_c^{-2} dependence of the cross sections. As seen from Fig. 7, the two-body part of the B1 cross sections rather accurately follows this law.

B. Three-body phenomena

A remarkable result of the spectral analysis is that the three-body part of the ionization process can be separated in good approximation from the two-body part (Fig. 6). At energies lower than about 200 eV, the spectral decomposition shows that the three-body part is well fitted by the extended dipole formula (10). At higher energies the separation of two- and three-body contributions becomes less reliable due to the interferences of different multipoles. In addition, the increasing statistical error of the data measured at forward and backward angles causes uncertainties in the determination of the three-body contribution (see the 500 eV spectrum). However, we estimated that the error of the three-body part does not exceed $\pm 40\%$ at the highest emitted electron energies.

As already noted, the extended dipole term contains contributions due to monopole transitions. These contributions include also the interference between monopole and dipole terms. The monopole term does not belong to the three-body part. Hence, the decomposition of the angular distributions is possible only if the monopole term is small. This is indeed shown in the following analysis.

It should first be recalled that the interferences between dipole and monopole terms cancel by integrating the cross sections over the electron emission angle. Hence it is useful to consider single-differential cross sections obtained after angular integration. Figure 7(b) shows integrated cross sections evaluated by means of the Born approximation (B1) code by Gulyás *et al.* [29]. The curve representing the monopole term (labeled ''B1:Monopole'') is seen to be relatively small. In fact, the summed dipole and monopole term (labeled ''B1:Dipole+Monopole'') is about an order of magnitude larger than the monopole term alone. Only at the highest energies near 1000 eV does the monopole term become important. The good agreement obtained between experiment and theory seen in Fig. 7(b) attests to the validity of attributing the fitted part of the experimental data to dipole transitions and, hence, to three-body effects.

Returning to the analogy between fast ions and photons, we note from the Einstein relation for the photoeffect that the present electron spectroscopy measurements allow for determining the energy of the annihilated (virtual) photon, since this photon energy is equal to the electronic energy transfer $\Delta E=\epsilon+E_b$ (recall that ϵ is the emitted electron energy and E_b is the binding energy). The probability for photoabsorption decreases strongly with photon energy following the power law $\Delta E^{-3.5}$ [14,35]. Therefore, we have fitted the experimental data with the function $x\Delta E^{-3.5}$, where x is a constant, which was adjusted to achieve agreement with the experimental data between 30 and 300 eV. The binding energy E_{1s} was used to determine ΔE, since the $1s$ orbital is governed by three-body effects (see the next subsection). The fit results given in Fig. 7(b) compare well with the results obtained from the Born approximation. The discrepancy at electron energies below 30 eV is due to the fact that the fit does not include the contribution from the $2s$ orbital, which gains importance at lower energies. At energies $\gtrapprox 300$ eV the discrepancy observed between the two theoretical data sets originates from the fact that the fit represent dipole transitions only, whereas the B1 results also include the monopole term.

Since the experimental three-body results imply the monopole term, it is expected that they agree primarily with the B1 curve. However, at higher energies the experimental data seem to follow the fit curve rather than the B1 curve. This disagreement is not fully understood at present. In any case, the important point to be made here is that the three-body part of ion-induced electron emission follows a $\Delta E^{-3.5}$ power law in accordance with the energy dependence of photoannihilation. The fact that photoabsorption and three-body processes follow the same energy dependence provides clear

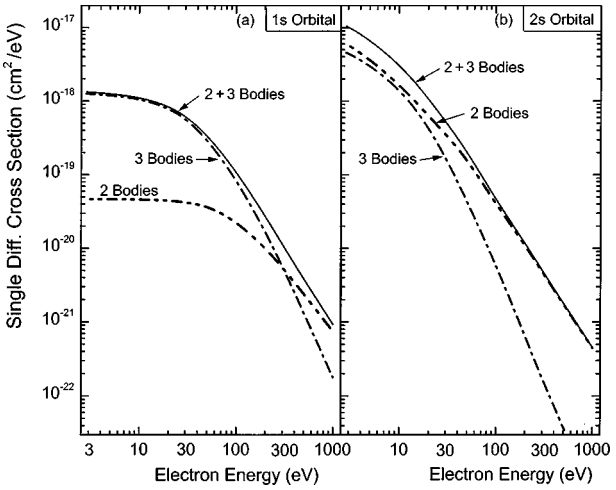

FIG. 8. Angle-integrated cross sections for electron emission in 95-MeV/u $Ar^{18+}+Li$ collisions divided into contributions from the $1s$ orbital (a) and the $2s$ orbital (b). All data were calculated using the Born approximation [29]. The curve labeled ''2 Bodies'' represents the multipoles $l \neq 1$ and the curve labeled ''3 Bodies'' represents the dipole $l=1$. The full line labeled ''2+3 Bodies'' refer to the sum of the individual contributions.

evidence for the analogy between ionization by photon and fast ion impact.

C. Shell contributions

As shown in the foregoing discussion, the decomposition of the experimental results provides information about two- and three-body effects. However, the experiment cannot distinguish the contributions of the $1s$ and $2s$ orbitals. Hence, to analyze these contributions we use theoretical cross sections evaluated by means of the Born approximation [29]. The excellent agreement found between experiment and theory in the foregoing analysis provides confidence that the theory also accurately predicts individual shell contributions.

The left- and right-hand sides of Fig. 8 present the partial cross sections for the $1s$ and $2s$ orbitals, respectively. Here, we have incorporated the monopole term into the two-body part so that the three-body part exclusively represents the dipole term (in accordance with Fig. 4). Also, the individual B1 cross sections for the $1s$ and $2s$ orbitals were found to compare well with results (not shown here) from the FEPA formula (14). This provides further confidence for the theoretical data presented here.

The results shown in Fig. 8 indicate that ionization of the $2s$ electron is most important at low energies whereas at higher energies the $1s$ ionization becomes dominant. Moreover, as already noted from Fig. 7, the two-body part governs the cross sections at high electron energies, since the three-body part decreases strongly with energy. This is due to the fact that the three-body cross section follows a power law with an exponent of -3.5 whereas the two-body part involves an exponent of -2 only.

The most significant result of the comparison of $1s$ and $2s$ contributions is that the two- and three-body effects are very different for the different shells. The $1s$ ionization is largely governed by three-body effects, i.e., two-body effects are found to be small in a wide range of lower electron energies. On the contrary, for the $2s$ orbital, two-body effects remain important even at the lowest electron energies studied here. Significant contributions of higher multipoles have been noted in the electron-loss cusp by Saábo *et al.* [36] As already noted from the spectra in Fig. 6, the observation of a significant two-body contribution at low electron energies is remarkable, since to date it is common practice to attribute the emission of soft-collision electrons to dipole transitions.

Indeed, the results for the Li $1s$ orbital (Fig. 8) support the dominance of the dipole transitions, i.e., at low energies the two-body part is found to be more than an order of magnitude lower than the three-body part. Similarly, in a recent study of He $1s$ ionization, Moshammer *et al.* [16] attributed soft-collision electrons uniquely to dipole transitions. However, the present results for the Li $2s$ orbital show that the conclusion of the dominant dipole contribution for soft-collision electrons cannot be generalized. Obviously specific properties of the $2s$ orbital favor the importance of two-body collisions or reduce the probabilities for three-body collisions. Characteristic properties of the $2s$ orbital are its small binding energy, its node producing an inner and outer part, and its large spatial extension. The analysis of the measured angular distributions (Figs. 5 and 6) has shown that the distinct part of the binary-encounter peak originates from the extensive outer portion of the $2s$ orbital. However, also the small $2s$ binding energy may influence the relation between the two- and three-body processes.

To find out which property of the $2s$ orbital has the dominant influence on the two- and three-body effects, we carried out auxiliary calculations using a (hydrogenic) $1s$ orbital with a binding energy of 5.5 eV. We note that the Li $2s$ orbital has the same binding energy but a diameter which is about a factor of 4 larger than this $1s$ orbital. The calculations show that the two-body cross sections for the $1s$ electron (bound with 5.5 eV) and the Li $2s$ electron are nearly equal. This can be understood from Eq. (16) indicating that the two-body cross section scales only with the binding energy. On the contrary, the three-body cross section, which is governed by the dipole form factor, strongly depends on the structure of the wave function (e.g., its node). The three-body cross section for the Li $2s$ orbital is found to be significantly reduced with respect to the results for the $1s$ orbital. Hence, the present observation that in soft collisions the three-body contribution of the Li $2s$ orbital does not dominate the two-body part is primarily caused by the structure of the $2s$ orbital.

Finally, in Fig. 9 we give an overview of the present analysis, which compares the experimental data with summed theoretical two- and three-body cross sections from Fig. 8. The two contributions are about equal at the lowest energy studied (3 eV), whereas at higher energies up to ~ 100 eV the three-body part exceeds the two-body part. At further increasing energy the three-body part drops rapidly so that the two-body part becomes dominant. As before, this is understood from the -3.5 power-law dependence of the three-body cross section which is much stronger than that of the two-body cross section.

V. CONCLUDING CONSIDERATIONS

We have shown for very fast projectiles colliding with Li that two- and three-body effects in single ionization can be

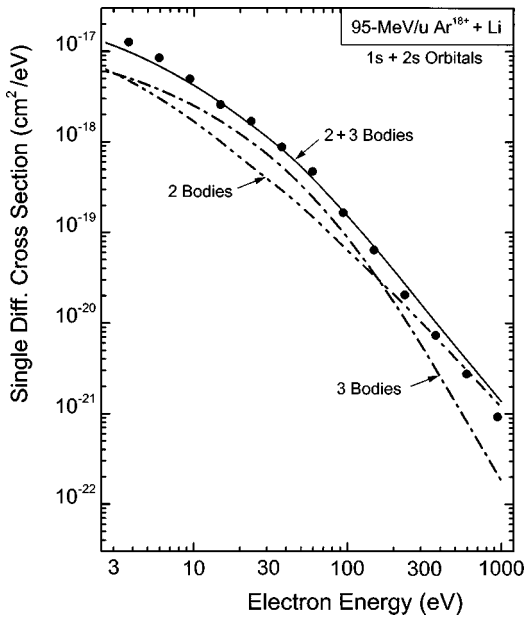

FIG. 9. Summary of angle-integrated cross sections for electron emission in 95-MeV/u $Ar^{18+}+Li$ collisions. The experimental data points, representing the sum of the data given in Fig. 7, were obtained by integrating the measured angular distributions. The theoretical results, referring to the sum of the 1*s* and 2*s* contributions, are obtained as in Fig. 8 where also the labels are specified.

separated. In the present analysis the use of high-energy projectiles is essential because (i) perturbation theory can be used, thus justifying the Born approximation, (ii) the minimum momentum transfer is very small so that the effect of soft collisions resembles photoannihilation, (iii) the binary encounter peak occurring near 90° has a particularly sharp profile, (iv) the monopole term is small and the $m=1$ term of the dipole transition is dominant, and (v) the interference between the monopole and dipole terms is small. Item (ii) constitutes the basis for the analogy between fast ions and photons.

In view of the present analysis, the question arises as to what are the limits for the separability of the two- and three-body processes which are associated with the multipole groups $l=1$ and $l\neq 1$, respectively. The basic condition for the separability of two- and three-body processes is that the different groups of multipoles appear in rather distinct regions of momentum transfer (Fig. 4). With decreasing electron energy the two groups approach each other and separability becomes more difficult. On the other hand, within the experimental analysis the angular distributions of the ejected electrons are exploited. This analysis indicates that two- and three-body effects are separable if the angular distribution exhibits a noticeable binary-encounter peak contribution, which is superimposed on the broad $(\sin^2\theta)$-like maximum attributed to three-body effects. A specific condition for analyzing the angular distributions is that interferences between dipole and higher multipoles are small. The present theoretical and experimental results show that separation of the multipole groups appears reasonable for electron energies as low as ~ 3 eV. Further studies below 3 eV would be needed to determine the limits for the separability of two- and three-body effects.

The theoretical analysis shows that two- and three-body effects play significantly different roles in the ionization of the Li 1*s* and 2*s* orbitals. Three-body effects are dominant for the removal of the 1*s* electron which contributes significantly to the total ionization at intermediate and higher energies. In Fig. 9 the relatively large three-body contributions near 30 eV originate primarily from the 1*s* ionization. On the contrary, the ionization of the 2*s* electron occurs predominantly via two-body interactions which are found to be important for electron energies as low as 3 eV. Therefore, in contrast to He, the two-body effects for Li remain significant for the soft collisions. This apparently strong two-body part is caused by the suppression of the three-body contribution, which in turn is due to the modal structure of the 2*s* orbital.

From the present findings the question arises as to how far the different conclusions for He or Li can be generalized to other target atoms. With its small binding energy and large extension the Li 2*s* orbital is rather unique. On the other hand, the He 1*s* orbital is also unique but its properties are opposite. Helium has the largest outer shell binding energy of any atom and a rather small extension. Hence, it appears promising to study the role of two-body effects for other target atoms having electrons in the 2*s* orbital or even higher shells whose binding energies lie between those of Li and He. From our results for the Li 2*s* orbital we would expect significant contributions from two-body effects for multishell atoms. However, to fully answer this question, further detailed work is required.

The fact that the experimental three-body data follow a $\Delta E^{-3.5}$ dependence shows that electron spectroscopy experiments with ion impact provide characteristic information about photoabsorption over a wide range of photon energies. It confirms the analogy of ionization by fast projectiles and photons which has attracted considerable attention in the past few years. It appears that even after so many decades of work in this field, originally started by Bethe [1], the analogy between ions and photons has not lost its fascination to researchers.

ACKNOWLEDGMENTS

We are indebted to Gregor Schiurets for helpful comments on the manuscript. This work was supported by the German-French Cooperation Program PROCOPE (Project No. 98089) and the German-Hungarian Intergovernmental Collaboration (Project No. B/129). J.-Y.C. received a grant from the Alexander von Humboldt Foundation, Germany; B.S. was supported by the Hungarian National Science Fund (Contract No. OTKA-T-020-771) and by the Hungarian Academic Research Fund (AKP, Contract No. 96/665 2,2); J.A.T. was supported by the Division of Chemical Sciences, Office of Basic Energy Sciences, Office of Energy Research, U.S. Department of Energy.

[1] H. A. Bethe, Ann. Phys. (Leipzig) **5**, 325 (1930).
[2] E. J. Williams, Phys. Rev. **45**, 325 (1934).
[3] M. E. Rudd, Y. K. Kim, D. H. Madison, and T. J. Gay, Rev. Mod. Phys. **64**, 441 (1992).
[4] N. Stolterfoht, R. D. Dubois, and R. D. Rivarola, *Electron Emission in Heavy Ion-Atom Collisions* (Springer-Verlag, Berlin, 1997).
[5] J. H. McGuire, *Introduction to Dynamic Correlation* (Cambridge University Press, Cambridge, 1997).
[6] U. Fano, Annu. Rev. Nucl. Sci. **13**, 1 (1963).
[7] M. Inokuti, Rev. Mod. Phys. **43**, 297 (1971).
[8] A. F. Starace, in *Atomic, Molecular, and Optical Physics Reference Book*, edited by G. W. F. Drake (American Institute of Physics, New York, 1996), Vol. 35.
[9] T. F. M. Bonsen and L. Vriens, Physica (Amsterdam) **47**, 307 (1970).
[10] J. N. Madsen and K. Taulbjerg, Phys. Scr. **T37**, 137 (1997).
[11] M. Inokuti, Y. Itakawa, and J. E. Turner, Rev. Mod. Phys. **50**, 23 (1978).
[12] Y.-K. Kim, Phys. Rev. A **6**, 666 (1972).
[13] Y.-K. Kim and M. Inokuti, Phys. Rev. A **7**, 1257 (1973).
[14] J. Burgdörfer, L. R. Anderson, J. H. McGuire, and T. Ishihara, Phys. Rev. A **50**, 349 (1994).
[15] Y. D. Wang, J. McGuire, J. Burgdörfer, and Y. Qiu, Phys. Rev. Lett. **77**, 1723 (1996).
[16] R. Moshammer *et al.*, Phys. Rev. Lett. **79**, 3621 (1997).
[17] L. Spielberger *et al.*, Phys. Rev. Lett. **74**, 4615 (1995).
[18] R. Dörner *et al.*, Phys. Rev. Lett. **77**, 1024 (1996).
[19] M. Gryzinski, Phys. Rev. **138**, A305 (1965); **138**, A332 (1965); **138**, A336 (1965).
[20] P. Eisenberger and P. M. Platzman, Phys. Rev. A **2**, 415 (1970).
[21] D. Brandt, Phys. Rev. A **27**, 1314 (1983).
[22] F. Bell, H. Böckl, M. Z. Wu, and H.-D. Betz, J. Phys. B **16**, 187 (1983).
[23] D. H. Lee *et al.*, Phys. Rev. A **41**, 4816 (1990).
[24] T. J. M. Zouros *et al.*, Phys. Rev. A **49**, 3155 (1994).
[25] B. Skogvall, M. Tschersisch, B. Sulik, J. Tanis, L. Gulyás, M. Grether, and N. Stolterfoht, Nucl. Instrum. Methods Phys. Res. B **124**, 186 (1997).
[26] N. Stolterfoht *et al.*, Phys. Rev. Lett. **80**, 4649 (1998).
[27] N. Stolterfoht, Z. Phys. **248**, 81 (1971).
[28] N. Stolterfoht *et al.*, in *Abstract of Contributed Papers*, edited by I. E. McCarthy, W. R. MacGillivray, and M. C. Standage (Griffith University Press, Bisbane, 1991), p. 393.
[29] L. Gulyás, P. D. Fainstein, and A. Salin, J. Phys. B **28**, 245 (1995).
[30] R. D. Cowan, *The Theory of Atomic Structure and Spectra* (University of California Press, Berkeley, CA, 1981).
[31] D. H. Madison, Phys. Rev. A **8**, 2449 (1973).
[32] S. T. Manson, L. H. Toburen, D. H. Madison, and N. Stolterfoht, Phys. Rev. A **12**, 60 (1975).
[33] J. P. Hansen and L. Kocbach, J. Phys. B **22**, L71 (1989).
[34] P. D. Fainstein, V. H. Ponce, and R. D. Rivarola, J. Phys. B **24**, 3091 (1991).
[35] T. Ishihara, K. Hino, and J. McGuire, Phys. Rev. A **44**, R6980 (1991).
[36] G. Szábo, J. Wang, and J. Burgdörfer, Phys. Rev. A **48**, R3414 (1993).